



# Photochemical synthesis of $\text{Co}_x\text{P}$ as cocatalyst for boosting photocatalytic $\text{H}_2$ production via spatial charge separation

Yuming Dong\*, Linggang Kong, Guangli Wang, Pingping Jiang, Na Zhao, Huizhen Zhang

Key Laboratory of Food Colloids and Biotechnology, School of Chemical and Material Engineering, Jiangnan University, Wuxi 214122, PR China



## ARTICLE INFO

### Article history:

Received 21 November 2016

Received in revised form 18 March 2017

Accepted 31 March 2017

Available online 2 April 2017

### Keywords:

Metal phosphide

Photochemical synthesis

Photocatalysis

Water splitting

Hydrogen generation

## ABSTRACT

Composed of earth-abundant elements, many metal phosphides have revealed remarkable advantages as photocatalytic hydrogen generation cocatalysts for their outstanding performance, stability and low cost. Taking the importance for solar energy utilization and current synthetic methods of metal phosphides into consideration together, we focus on the safe and energy-saving preparation of metal phosphide as cocatalyst for photocatalytic hydrogen evolution. Herein, taking  $\text{Co}_x\text{P}/\text{CdS}$  as a case, a novel photochemical strategy to synthesize  $\text{Co}_x\text{P}$  is proposed and realized. In this process, Co salt and  $\text{NaH}_2\text{PO}_2$  are used as the source of Co and P, and the typical preparation of  $\text{Co}_x\text{P}$  can be completed within 1 h. Furthermore, the optimized hydrogen evolution rate of  $\text{Co}_x\text{P}/\text{CdS}$  is about  $500 \text{ mmol g}^{-1} \text{ h}^{-1}$  under visible light, which is one of the most robust photocatalytic HER systems currently. Besides, the photocatalytic  $\text{H}_2$  evolution mechanism using  $\text{Co}_x\text{P}$  as cocatalyst is also proposed, where  $\text{Co}_x\text{P}$  can effectively prevent the recombination of photogenerated electrons and holes. The photochemical synthesis route opens a door for facile preparation and practical application of many other metal phosphides.

© 2017 Elsevier B.V. All rights reserved.

## 1. Introduction

From the view of both environmental protection and energy dilemma, the development of renewable energy is of great significance. Hydrogen energy has received growing attention as an environment-friendly fuel. Since the concept of photocatalytic water-splitting was proposed [1], sunlight-driven hydrogen evolution reaction (HER) has been considered to be a sustainable way of energy production. During past 40 years, various photocatalytic systems have been developed for hydrogen generation from water [2–4]. Based on great progresses and efforts which have been made, there are still several challenging issues such as low quantum efficiency, poor stability or expensive materials. Up to now, robust and commercially available photocatalytic systems are still greatly desirable.

Composed of earth-abundant elements, many metal phosphides are known for their stability and low cost. In 2005, the possibility of metal phosphide ( $\text{Ni}_2\text{P}$ ) as highly active HER catalyst was firstly predicted by density functional theory calculations [5]. Since 2013, metal phosphides used as HER electrocatalysts have been reported and revealed outstanding performance, including low

over-potential and excellent durability under conditions of wide pH range [6,7]. Many excellent electrocatalytic HER processes based on metal phosphides were developed, such as  $\text{FeP}$  [8,9],  $\text{CoP}$  and  $\text{Co}_2\text{P}$  [10–13],  $\text{Ni}_2\text{P}$  and  $\text{Ni}_5\text{P}_4$  [14–17],  $\text{MoP}$  [18] and  $\text{Cu}_3\text{P}$  [19]. These works indicate promising applications of metal phosphides in HER and the electrocatalytic performances were approved by theoretical calculations again [6]. From 2014, transition metal (Fe, Co, Ni and Cu) phosphides were proposed as efficient co-catalysts for photocatalytic hydrogen generation [9,20–26]. For example, the hydrogen-production rate can reach up to  $254 \text{ mmol h}^{-1} \text{ g}^{-1}$  under sunlight irradiation through the  $\text{CoP}-\text{CdS}$  hybrid photocatalyst proposed by Yong Chen and Wen-Fu Fu's Group, and a high hydrogen-production rate of  $1200 \text{ } \mu\text{mol h}^{-1} \text{ mg}^{-1}$  was obtained under visible light irradiation based on the  $\text{Ni}_2\text{P}-\text{CdS}$  hydrogen evolution photocatalyst designed by Pingwu Du's Group. Furthermore, in a more recent paper [27], the photoexcited electrons transfer from photo-active material ( $\text{CdS}$ ) to metal phosphide ( $\text{Co}_2\text{P}$ ) was investigated in detail by spectroscopic characterizations and theoretical calculations. These great works revealed remarkable advantages of metal phosphides as sunlight-driven hydrogen generation cocatalysts.

As for the synthesis of metal phosphides as HER catalyst, there are four main routes according to the difference of phosphorus source. The first one is solution phase synthesis at elevated temperature ( $>300^\circ\text{C}$ ) in organic solvent using tri-*n*-octylphosphine (TOP)

\* Corresponding author.

E-mail addresses: [dongym@jiangnan.edu.cn](mailto:dongym@jiangnan.edu.cn), [dongyuming1981@163.com](mailto:dongyuming1981@163.com) (Y. Dong).

as phosphorus source [8–12,14,15,17,20,23,27], which is highly flammable and corrosive. The second method is phosphorization by  $\text{PH}_3$ , which is extremely toxic and can be *in situ* generated by thermal decomposition of hypophosphites (such as  $\text{NaH}_2\text{PO}_2$ ) at a high temperature about 300–400 °C. [10,13,19,21,24,26] The third route is phosphorization under hydrothermal conditions at about 140–200 °C by elemental phosphorus including white, yellow and red phosphorus. [16,22,25,27] And the forth strategy is the reduction of metal orthophosphates by  $\text{H}_2$  at high temperature (>600 °C), in which phosphate group acts as the phosphorus source [6,18]. These classical methods have played key and significant roles for development of metal phosphides as HER catalysts [7]. At the same time, from the view of safe and energy saving synthesis, it is greatly necessary and significant to design novel preparation strategy for metal phosphides.

Taking the importance for solar energy utilization and current synthetic methods of metal phosphides into consideration together, we focus on the rapid and facile preparation of metal phosphide as cocatalyst for photocatalytic HER.  $\text{CdS}$  is one of the most attractive photocatalytic materials for the conversion of solar energy into hydrogen energy, and  $\text{CdS}$  nanorods (NRs) represent excellent photocatalytic activity of  $\text{H}_2$  evolution under visible light [22,23,27]. Herein, taking  $\text{Co}_x\text{P}/\text{CdS}$  as a case, we proposed a novel photochemical strategy to synthesize  $\text{Co}_x\text{P}$  at room temperature. In this process, Co salt and  $\text{NaH}_2\text{PO}_2$  were used as the source of Co and P, and the typical preparation of  $\text{Co}_x\text{P}$  can be completed within 1 h. Furthermore, the optimized hydrogen evolution rate of as-prepared  $\text{Co}_x\text{P}/\text{CdS}$  was about 500  $\text{mmol g}^{-1} \text{h}^{-1}$  under visible light, which is one of the most robust photocatalytic HER systems currently. To the best of our knowledge, as a mild and rapid synthesis method, photochemical strategy used for the preparation of metal phosphide has not been reported. Our work provides a novel and safe route for preparation of metal phosphide as a highly efficient cocatalyst for photocatalytic hydrogen evolution.

## 2. Experimental section

### 2.1. Preparation of $\text{CdS}$ NRs

All reagents were purchased from Sinopharm Chemical Reagent Co. Ltd. and used without further purification.  $\text{CdS}$  NRs were prepared using a modified method which was reported by previous literatures [22,29]. In a typical synthesis, 20.25 mmol  $\text{CdCl}_2 \cdot 2.5\text{H}_2\text{O}$  and 60.75 mmol  $\text{NH}_2\text{CSNH}_2$  were dispersed in 60 mL ethylenediamine and then transferred to a 100 mL Teflon-lined stainless-steel autoclave, which was later maintained at 160 °C for 48 h and then allowed to cool down to room temperature. The yellow precipitate was washed with absolute ethanol and distilled water and then dried at 60 °C in a vacuum drying.

### 2.2. Synthesis of $\text{Co}_x\text{P}/\text{CdS}$ NRs composite

The  $\text{Co}_x\text{P}/\text{CdS}$  NRs composite was prepared by a photochemical method. Briefly, 50 mg of  $\text{CdS}$  NRs, 2 mL of  $\text{CoCl}_2$  (0.1 M) aqueous solution, 7 mL of  $\text{NaH}_2\text{PO}_2$  (0.2 M) aqueous solution and 1 mL of  $\text{H}_2\text{O}$  were mixed in a 40 mL flask at ambient temperature. Then the mixed system was purged by pure nitrogen for 40 min. Subsequently, the mixture was illuminated under UV-vis light (300 W Xe lamp). After illumination, the precipitate was washed with distilled water to remove the residues of reagents and dried under  $\text{N}_2$  flowing. The deposition content of  $\text{Co}_x\text{P}$  can be adjusted by changing illumination time. The obtained products were named as  $\text{Co}_x\text{P-T}/\text{CdS}$  NRs, where T referred to the illumination time (min) under UV-vis light.

### 2.3. Photocatalytic hydrogen production

The photocatalytic experiments were performed in a 260 mL reactor (Fig. S2) at ambient temperature. A 300 W Xe lamp with 420 nm cut-off filter was employed as the light source. The as-prepared  $\text{Co}_x\text{P-T}/\text{CdS}$  NRs sample was added to aqueous solution containing sacrificial agent. After sonication for 5 min, the mixture was purged by a nitrogen gas for 1 h. The generated hydrogen was measured by gas chromatography (GC-9790, argon as a carrier gas) using a 5 Å molecular sieve column and a thermal conductivity detector (TCD).

### 2.4. Characterization

To confirm the composition and phase of the sample, X-ray diffraction (XRD) patterns were recorded on a D8 X-ray diffractometer (Bruker AXS, German). Size and lattice fringe measurements were analyzed by transmission electron microscope (TEM) using JEM-2100 transmission electron microscope (JEOL, Japan), and energy-dispersive X-ray spectroscopy (EDX) was taken on the TEM instrument (Fig. S3). The EDX-mapping images were obtained with a Tecnai G2 F30 transmission electron microscope (FEI, USA) equipped with a Rontec EDX system (Figs. 2 and S15). An environmental scanning electron microscope (Hitachi S-4800) coupled with an energy-dispersive X-ray spectroscope (SEM/EDX) was also employed to investigate microscopic feature. The X-ray photoelectron spectroscopy (XPS) analysis was conducted using an ESCALAB 250 Xi (Thermo, USA) X-ray photoelectron spectrometer with  $\text{Al K}\alpha$  as the excitation source ( $\hbar\nu = 1484.6$  eV). UV-vis absorption spectra were measured using a spectrophotometer (Shimadzu, Japan UV-3600 Plus). Photoluminescence (PL) measurements were carried out on a CARY Eclipse (Varian, USA) fluorescence spectrophotometer. The surface photovoltage (SPV) was determined for investigating charges features by self-made equipment [33,34]. Electrochemistry measurements were performed by a CHI660E electrochemical analyzer (Chenhua Instruments Co., China), with  $\text{Ag}/\text{AgCl}$  electrode used as reference electrode, Pt wire employed as the counter electrode, and glassy carbon electrode served as the working electrode.

## 3. Results and discussion

### 3.1. Characterization of $\text{Co}_x\text{P}/\text{CdS}$

Firstly, control experiments were designed to investigate the influence of the preparation time (irradiation time under UV-vis light) of  $\text{Co}_x\text{P}/\text{CdS}$  on the catalytic activity. Fig. S1 showed the photocatalytic HER activity of different  $\text{Co}_x\text{P-T}/\text{CdS}$  samples (T referred to the illumination time (min)), which were obtained by the reactor shown in Fig. S2. With the preparation time increased from 0 to 50 min, the  $\text{H}_2$  production rate increased from 0.22  $\text{mmol g}^{-1} \text{h}^{-1}$  to 18.9  $\text{mmol g}^{-1} \text{h}^{-1}$  (enhanced about 85 times than pure  $\text{CdS}$ ), which was due to the increasing content of  $\text{Co}_x\text{P}$ . However, the hydrogen evolution rate gradually declined when the illumination time was over 50 min, because overloading of  $\text{Co}_x\text{P}$  could decrease the oxidation reaction sites on the surface of  $\text{CdS}$  NRs [28]. The results demonstrate that  $\text{Co}_x\text{P}$  was an effective co-catalyst for  $\text{CdS}$  NRs and 50 min was proper for preparation of  $\text{Co}_x\text{P}/\text{CdS}$  composite. Therefore, the photochemical preparation time of  $\text{Co}_x\text{P}/\text{CdS}$  was set as 50 min in next experiments.

XRD was used to confirm the composition of pure  $\text{CdS}$  NRs and  $\text{Co}_x\text{P-50}/\text{CdS}$  hybrid photocatalysts. As shown in Fig. 1, all the diffraction peaks of  $\text{Co}_x\text{P-0}/\text{CdS}$  are matched with the standard cards of  $\text{CdS}$  (JCPDS 77-2306). The reflections of  $\text{Co}_x\text{P-50}/\text{CdS}$  were indexed to the hexagonal phase  $\text{CdS}$  [29], and there is no obvious

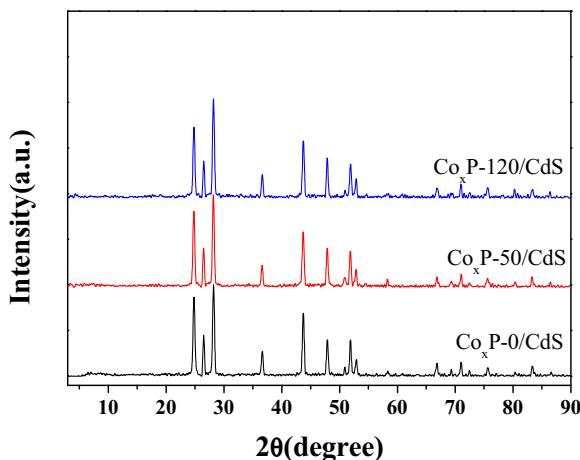


Fig. 1. XRD patterns of  $\text{Co}_x\text{P-0/CdS}$ ,  $\text{Co}_x\text{P-50/CdS}$  and  $\text{Co}_x\text{P-120/CdS}$ .

diffraction peaks of  $\text{Co}_x\text{P}$  in the XRD patterns. Even the preparation time was prolonged to 120 min, the XRD results of  $\text{Co}_x\text{P-120/CdS}$  were similar with that of  $\text{Co}_x\text{P-50/CdS}$ , suggesting that the  $\text{Co}_x\text{P}$  is probably amorphous structure.

The morphology, elemental and spatial distribution of the atoms with  $\text{Co}_x\text{P-50/CdS}$  hybrid photocatalysts were investigated by EDX-Mapping, SEM/EDX and TEM/EDX. The EDX-Mapping images (Fig. 2a) show that, both Co and P elements are uniformly distributed throughout the nanoparticle, while both Cd and S elements are uniformly distributed throughout on nanorods. The results were coincident with the results of TEM/EDX (Fig. S3). All the ele-

ment of Cd, S, Co and P can be found according to the results of SEM/EDX (Fig. 2b). These results indicated the existence of  $\text{Co}_x\text{P}$  nanoparticles on CdS nanorods. And as shown in Figs. 2c and S3–S4, the CdS NRs have average length of about 600 nm and diameter of about 35 nm, and the  $\text{Co}_x\text{P}$  nanoparticles linked with the surface of CdS NRs. The HRTEM image (Fig. 2d) shows the lattice fringes of CdS and  $\text{Co}_2\text{P}$ . The inter planar spacing of 0.31 nm is consistent with the spacing of (101) planes of CdS, and that of 0.221 nm is consistent with the spacing of (121) planes of  $\text{Co}_2\text{P}$ . Furthermore, the SEM/EDX results of several  $\text{Co}_x\text{P-T/CdS}$  samples were determined and listed in Table S1. It can be found that the atom ratios of Co/P are between 1.1–1.6, and then the composition of  $\text{Co}_x\text{P}$  was concluded as the mixture of CoP and  $\text{Co}_2\text{P}$ . Furthermore, the contents of Co and P in  $\text{Co}_x\text{P-50/CdS}$  are 2.25 wt% and 0.99 wt%, respectively (measured by ICP-MS). Then the total content of  $\text{Co}_x\text{P}$  is calculated as about 3.3 wt% in  $\text{Co}_x\text{P-50/CdS}$  with Co/P mole ratio of 1.16 (between 1.1–1.6).

The composition and chemical status of Co and P element in  $\text{Co}_x\text{P-50/CdS}$  were investigated by X-ray photoelectron spectroscopy (XPS). For Co 2p (Fig. 3a), three peaks appeared in the region at 786.5, 781.9 and 778.6 eV. The peak at 778.6 eV is positively shifted from that of Co metal (777.9 eV), suggesting the presence of reduced Co species in  $\text{Co}_x\text{P}$  [23,35,36]. And the peak at 781.9 eV as well as the satellite peak (at ca. 786.5 eV) correspond to Co (+II) and are consistent with previous reports [36,37]. As shown in Fig. 3b, the peaks at 129.9 and 130.4 eV indicated the formation of cobalt phosphide, and the peak at 133.5 eV can be assigned to surface metal phosphate species [23,25,36]. Moreover, the binding energy of Cd 3d (Fig. 3c) and S 2p (Fig. 3d) are matched well with that of CdS [22].

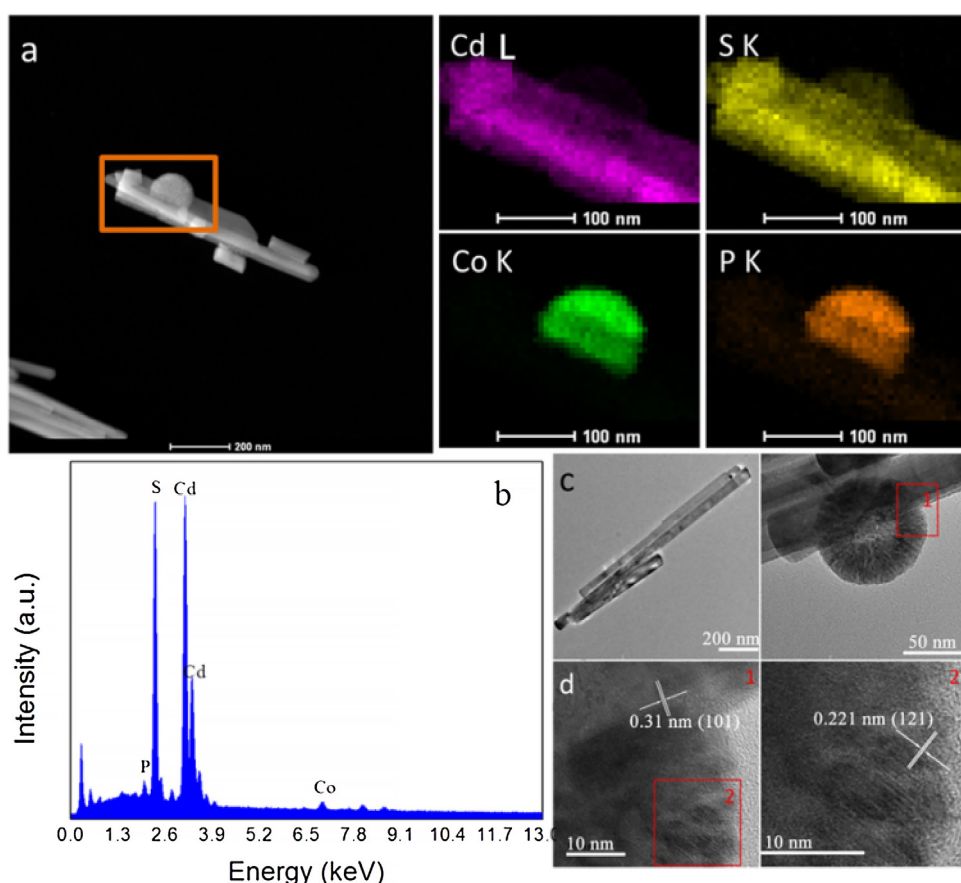
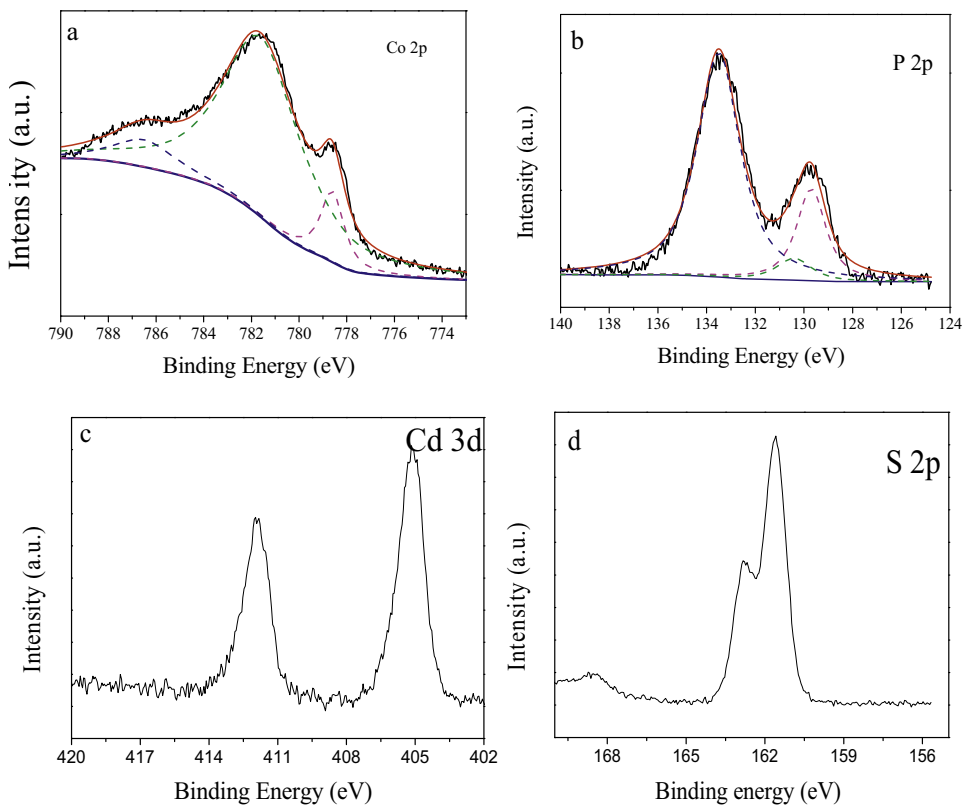


Fig. 2. (a) EDX-Mapping images for cadmium, sulfur, cobalt and phosphorus elements in  $\text{Co}_x\text{P-50/CdS}$ ; (b) SEM/EDX results of  $\text{Co}_x\text{P-50/CdS}$ ; (c) TEM and (d) HRTEM images of  $\text{Co}_x\text{P-50/CdS}$ .



**Fig. 3.** High-resolution XPS spectra of  $\text{Co}_x\text{P-50/CdS}$ . (a) Co 2p of  $\text{Co}_x\text{P}$ , (b) P 2p of  $\text{Co}_x\text{P}$ , (c) Cd 3d of CdS, (d) S 2p of CdS.

**Table 1**  
Preparation conditions for control experiments.

	CdS NRs /mg	$\text{CoCl}_2$ (0.1 M)/mL	$\text{NaH}_2\text{PO}_2$ (0.2 M) /mL	Water/mL	Irradiation time /min
A	50	2	7	1	Dark 50
B	50	0	7	3	50
C	50	2	0	8	50
D	50	2	7	1	50
E	0	2	7	1	50

### 3.2. Photochemical formation of $\text{Co}_x\text{P}$

Control experiments were carried out to investigate the effect of various conditions on the photochemical formation of  $\text{Co}_x\text{P}$ . The experimental conditions were set as shown in Table 1. Experiment D is the typical preparation of  $\text{Co}_x\text{P-50/CdS}$ , including CdS,  $\text{CoCl}_2$ ,  $\text{NaH}_2\text{PO}_2$  and irradiation for 50 min under UV-vis light. In experiment A, the same mixture as that in experiment D was treated under dark (without irradiation of light) for 50 min. In experiment B, the mixture including CdS and  $\text{NaH}_2\text{PO}_2$  was treated for 50 min under UV-vis light, and the difference from experiment D is the absence of  $\text{CoCl}_2$ . In experiment C, the mixture including CdS and  $\text{CoCl}_2$  was treated for 50 min under UV-vis light, and the difference from experiment D is the absence of  $\text{NaH}_2\text{PO}_2$ . In experiment E, the mixture including  $\text{CoCl}_2$  and  $\text{NaH}_2\text{PO}_2$  was treated for 50 min under UV-vis light, and the difference from experiment D is the absence of CdS. After 50 min of treatment, the solid samples from A, B, C and D were washed and dried according to the same procedure as  $\text{Co}_x\text{P-50/CdS}$ , respectively. And no solid was observed and obtained from experiment E, indicating the unique role of photo-active material. Then the photocatalytic hydrogen evolution activity of the solid catalyst obtained from experiment A–D were tested and the amounts of hydrogen were shown in Fig. 4. It can be found that the  $\text{H}_2$  evolution rate of sample D (1326.7  $\text{mmol g}^{-1}$ ) during 8 h was much

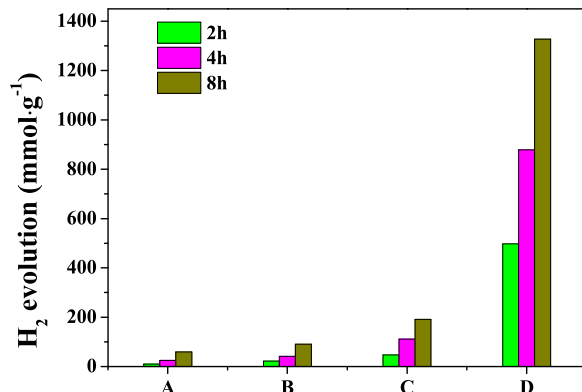


**Fig. 4.** Comparison of the photocatalytic activity of samples obtained according to preparation conditions in Table 1. This photocatalytic  $\text{H}_2$  evolution system contained 3 mg of sample and 50 mL 10 vol% lactic acid aqueous solution, under 300 W Xe lamp with 420 nm cut-off filter for 8 h.

higher than that of sample A (59.3  $\text{mmol g}^{-1}$ ), B (89.9  $\text{mmol g}^{-1}$ ) and C (191.3  $\text{mmol g}^{-1}$ ). As shown in Fig. 2b, both Co and P can be found in sample D ( $\text{Co}_x\text{P-50/CdS}$ ). From the results of SEM/EDX (Fig. S5), neither cobalt nor phosphorus element was observed in sample A, denoting the necessity of irradiation. At the same time, only trace amount of P was observed in sample B and small amount of Co was found in sample C by the results of SEM/EDX (Figs. S6 and S7). Therefore, for the photosynthesis of efficient cocatalyst  $\text{Co}_x\text{P}$ , all of photo-active material (such as CdS), cobalt salt (such as  $\text{CoCl}_2$ ), proper phosphorus source hypophosphites (such as  $\text{NaH}_2\text{PO}_2$ ) and irradiation are essential and necessary.

As known, with middle valence state of phosphorus, hypophosphites reveal reduction performance and oxidation property at the same time. For instance,  $\text{NaH}_2\text{PO}_2$  can undergo thermal decomposition to  $\text{P}(-\text{III})$  and  $\text{P}(+\text{V})$  at elevated temperature about 300–400 °C.

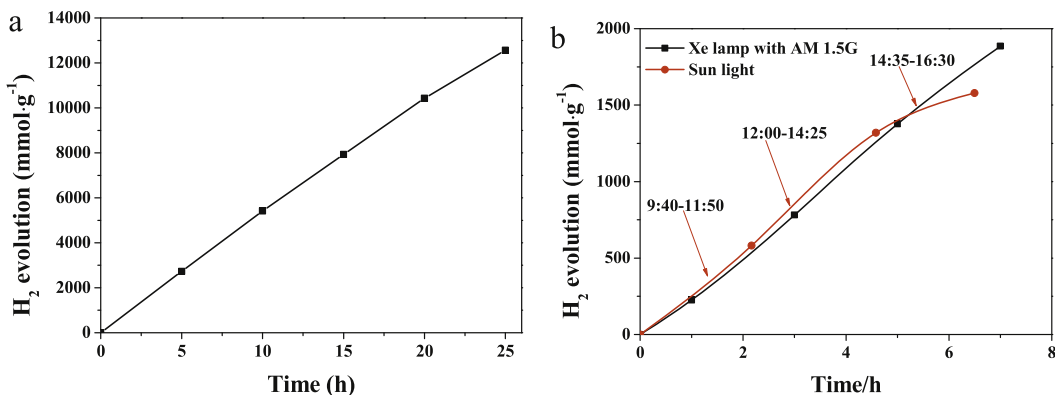
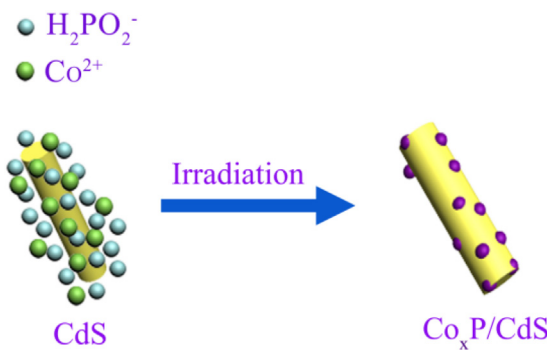
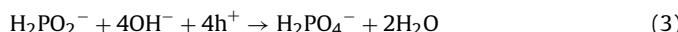
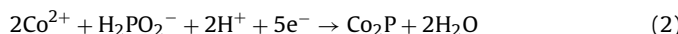


**Fig. 5.** (a) The amount of H<sub>2</sub> evolution with 1 mg Co<sub>x</sub>P-50/CdS in 50 mL 1.25 M/1.75 M of Na<sub>2</sub>S/Na<sub>2</sub>SO<sub>3</sub> aqueous solution under 300 W Xe lamp with 420 nm cut-off filter. (b) Photocatalytic hydrogen evolution under 300 W Xe lamp with AM 1.5G filter and sunlight irradiation in Wuxi city on March 28, 2016. Outdoor temperature: 9–19 °C, time: 9:40–16:30. The system contained 2 mg Co<sub>x</sub>P-50/CdS in 50 mL of 0.75 M/1.05 M Na<sub>2</sub>S/Na<sub>2</sub>SO<sub>3</sub> aqueous solution.



**Scheme 1.** Proposed photochemical synthesis route of cobalt phosphide in Co<sub>x</sub>P/CdS.

Under irradiation, the photo-active material (such as CdS) adsorbed light and produced hole-electron pairs. The photogenerated electrons and holes were subsequently transported to the surface. Under this condition, part of H<sub>2</sub>PO<sub>2</sub><sup>-</sup> were reduced by the electrons and others were oxidized by the holes meanwhile. In presence of Co<sup>2+</sup>, corresponding equations were concluded as following:



Are the holes on valence band (VB) and electrons on conductive band (CB) of CdS proper for above reactions? In order to prove the feasibility of above equations, the current-potential curve (J-V) of the clear solution (without CdS) in experiment B, C and D were investigated. From Fig. S8, the reduction potential of pure Co<sup>2+</sup> was determined as -0.928 V vs NHE and that of pure H<sub>2</sub>PO<sub>2</sub><sup>-</sup> was -0.884 V vs NHE. When Co<sup>2+</sup> and H<sub>2</sub>PO<sub>2</sub><sup>-</sup> were mixed, the reduction potential moved to -0.712 V vs NHE. The results indicated that, although both Co<sup>2+</sup> and H<sub>2</sub>PO<sub>2</sub><sup>-</sup> can be reduced under certain potential, the formation of Co<sub>x</sub>P was prior. The conclusion is coincident with the photochemical reaction results in Table 1. The results were also coincident with the electrochemical preparation of cobalt phosphide by reduction process [30]. Furthermore, the oxidation potential and reduction potential of the mixture of Co<sup>2+</sup> and H<sub>2</sub>PO<sub>2</sub><sup>-</sup> match well with the VB and CB of CdS NRs [22,29]. Base on these experimental results, the photochemical synthesis route of cobalt phosphide can be described as shown in Scheme 1.

### 3.3. Photocatalytic performance and mechanism

Light absorption is the first step for the utilization of solar energy. The light-absorption properties were measured by UV-vis-diffuse reflectance spectra and the results are shown in Fig. S9. All the absorption edges of Co<sub>x</sub>P-0/CdS, Co<sub>x</sub>P-50/CdS and Co<sub>x</sub>P-120/CdS are around 520 nm, which indicates that the absorption edge of CdS is not shifted after loading of Co<sub>x</sub>P. However, the absorption level is enhanced in the visible light region after 520 nm, indicating that Co<sub>x</sub>P is tightly deposited on the surface of CdS NRs [22].

Then, the influence of hole scavenger on the HER rate of Co<sub>x</sub>P-50/CdS photocatalyst was investigated. In this experiment, the aqueous solution of methanol, triethanolamine, lactic acid and Na<sub>2</sub>S/Na<sub>2</sub>SO<sub>3</sub> were prepared respectively and compared together. As shown in Fig. S10, Co<sub>x</sub>P-50/CdS photocatalyst revealed higher activity when lactic acid and Na<sub>2</sub>S/Na<sub>2</sub>SO<sub>3</sub> were used as sacrificial agent. However, with the illumination time increasing, the rate of H<sub>2</sub> evolution gradually decreased in 10 vol% lactic acid aqueous solution, because the cadmium sulfide is unstable in acidic environment [20]. Compared with that in methanol, triethanolamine and lactic acid, the rate of H<sub>2</sub> evolution in Na<sub>2</sub>S/Na<sub>2</sub>SO<sub>3</sub> aqueous solution is high and stable. Therefore, Na<sub>2</sub>S/Na<sub>2</sub>SO<sub>3</sub> was employed as a hole scavenger in next experiments. In addition, the influence of Na<sub>2</sub>S/Na<sub>2</sub>SO<sub>3</sub> concentrations on the photocatalytic activity of Co<sub>x</sub>P/CdS photocatalyst has been investigated and showed in Fig. S11. With the concentration of hole scavenger increased from 0.25 M/0.35 M to 1.5 M/2.1 M, the H<sub>2</sub> evolution rate increased gradually. The maximum H<sub>2</sub> evolution rate is about 405 mmol h<sup>-1</sup> g<sup>-1</sup>. The results showed that a higher concentration of hole scavenger led to faster transfer of the photogenerated holes and suppressed the recombination of photogenerated electron-hole [31].

Focus on practical application, stability and durability are indispensable for an excellent photocatalyst. In order to evaluate the stability of the Co<sub>x</sub>P-50/CdS, we performed a long time hydrogen production experiment under 300 W Xe lamp with 420 nm cut-off filter. Fig. 5a shows the H<sub>2</sub> production as a function of irradiation time. During irradiation for 25 h, the total H<sub>2</sub> amount of Co<sub>x</sub>P-50/CdS reached up to 12600 mmol g<sup>-1</sup>, denoting a stable photocatalytic activity of about 504 mmol g<sup>-1</sup> h<sup>-1</sup>. As known, noble metal Pt is an efficient hydrogen evolution cocatalyst for many semiconductors. We further tested the photocatalytic hydrogen production activity of 0.5 wt% and 3.3 wt% Pt/CdS for comparison under the same conditions (Fig. S12). This result shows that the photocatalytic H<sub>2</sub> evolution rate of 0.5 wt% and 3.3 wt% Pt/CdS is about 225 and 167 mmol g<sup>-1</sup> h<sup>-1</sup>, which is less than that of Co<sub>x</sub>P-50/CdS

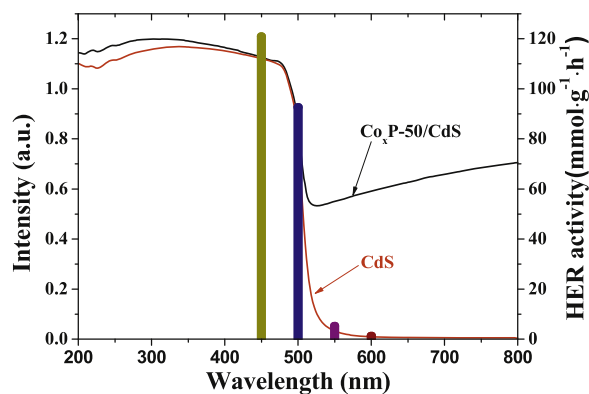
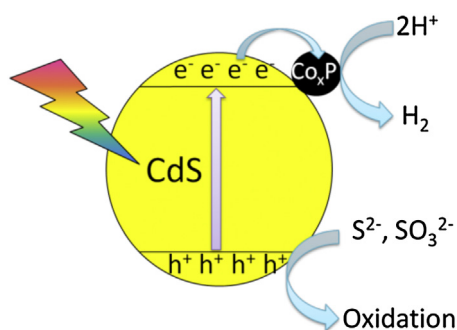


**Fig. 6.** UV-vis-diffuse reflectance spectra and the HER activity of  $\text{Co}_x\text{P-50/CdS}$  under light of certain wavelength. This system contained 3 mg of sample in 50 mL of 0.75 M/1.05 M  $\text{Na}_2\text{S}/\text{Na}_2\text{SO}_3$  aqueous solution, and 300 W Xe lamp with band-pass filter of different wavelength was employed as the light source.

(545  $\text{mmol g}^{-1} \text{h}^{-1}$ ). According to the reported results summarized in Table S2,  $\text{Co}_x\text{P-50/CdS}$  is among the most robust HER photocatalysts. When we carried out the photocatalytic HER experiments, obvious bubbles can be observed by naked eyes and shown in supporting information II (a separate AVI file). After photocatalytic HER for 25 h, the  $\text{Co}_x\text{P-50/CdS}$  catalyst was characterization again by XRD, TEM and EDX mapping (Figs. S13–S15), and no obvious change was observed. These results indicate that the prepared  $\text{Co}_x\text{P-50/CdS}$  is durable for photocatalytic  $\text{H}_2$  production from water and  $\text{Co}_x\text{P}$  is an outstanding HER cocatalyst in present system.

The most fundamental objective of photocatalysis is the high-efficiency application of solar energy. Then hydrogen production experiments were carried out under nature sunlight outdoors (Fig. S16) and 300 W Xe lamp with AM 1.5G filter irradiation, respectively. As the results shown in Fig. 5b, the  $\text{H}_2$  production rate was about 1580  $\text{mmol g}^{-1}$  after sunlight irradiation for 6.5 h, and HER activity of 1890  $\text{mmol g}^{-1}$  was obtained during irradiation of 7 h under 300 W Xe lamp with AM 1.5G filter. These results indicated that  $\text{Co}_x\text{P-T/CdS}$  was a robust photocatalyst for sunlight-driven  $\text{H}_2$  production from water.

Compared with pure  $\text{CdS}$ ,  $\text{Co}_x\text{P-50/CdS}$  revealed stronger absorption for visible light (Fig. S9). Is the enhanced absorption of visible light responsible for the remarkable photocatalytic activity of  $\text{Co}_x\text{P-50/CdS}$ ? To answer this question, a control experiment was designed and the results were shown in Fig. 6. The photocatalytic activity of  $\text{H}_2$  evolution along with wavelength coincided well with the UV-vis absorption spectrum of pure  $\text{CdS}$ , not that of  $\text{Co}_x\text{P-50/CdS}$ . The results indicated that the enhanced absorption in the visible region from  $\text{Co}_x\text{P}$  contributed hardly to the high photocat-



**Scheme 2.** Proposed photocatalytic  $\text{H}_2$  production mechanism of  $\text{Co}_x\text{P/CdS}$ .

alytic activity of  $\text{Co}_x\text{P-50/CdS}$ . The results well demonstrated the cocatalyst role of  $\text{Co}_x\text{P}$  in this hybrid photocatalyst.

In order to investigate the reason for enhanced photocatalytic activity of  $\text{Co}_x\text{P-50/CdS}$ , we performed the photoluminescence (PL) spectra, which is able to reflect the transfer of photogenerated charge carriers. Fig. 7a presents the PL spectra of  $\text{Co}_x\text{P-50/CdS}$  with an excitation wavelength of 385 nm, and distinct emission bands at about 530 nm can be observed. The PL emission intensity of  $\text{Co}_x\text{P-0/CdS}$  is about 6 times higher than that of  $\text{Co}_x\text{P-50/CdS}$ . This is due to the fast transfer of electrons from  $\text{CdS}$  to  $\text{Co}_x\text{P}$ , which can suppress the recombination of electron–hole and enhance the photocatalytic activity. In addition, as shown in Fig. 7b, surface photovoltage (SPV) spectrum was determined to study the photogenerated charge separate efficiency of  $\text{CdS}$  and  $\text{Co}_x\text{P-50/CdS}$ . Both  $\text{Co}_x\text{P-50/CdS}$  and pure  $\text{CdS}$  revealed an obvious positive photovoltage response in the range of 300–550 nm. This result indicated again that the band gap of  $\text{CdS}$  was not changed after loading of  $\text{Co}_x\text{P}$ , which is coincident with the results in Fig. S9. The photovoltage response intensity of  $\text{Co}_x\text{P-50/CdS}$  increased obviously compared with pure  $\text{CdS}$ , which demonstrated a higher charge separation efficiency. Furthermore, the photocurrent response of  $\text{Co}_x\text{P-50/CdS}$  is higher than that of pure  $\text{CdS}$  NRs (Fig. S17). The higher photocurrent of  $\text{Co}_x\text{P-50/CdS}$  suggested enhanced efficiency in separation of the photogenerated electron–hole pairs. All the results from the PL, SPV and photoelectrochemical (PEC)  $I-t$  curves indicate that the separation efficiency of photogenerated carriers of  $\text{CdS}$  can be effectively enhanced by  $\text{Co}_x\text{P}$ .

**Scheme 2** shows the proposed photocatalytic  $\text{H}_2$  evolution mechanism for the  $\text{Co}_x\text{P/CdS}$  heterostructures. Under visible light irradiation, the  $\text{CdS}$  NRs were excited, and then electrons–holes were generated. With the modification of  $\text{Co}_x\text{P}$ , the photogenerated electrons in the conduction band of  $\text{CdS}$  are very easy to be transferred to  $\text{Co}_x\text{P}$ . Therefore, the electron–hole recombination trends in  $\text{CdS}$  are weakened. The trapped electrons at the  $\text{Co}_x\text{P}$  can eas-

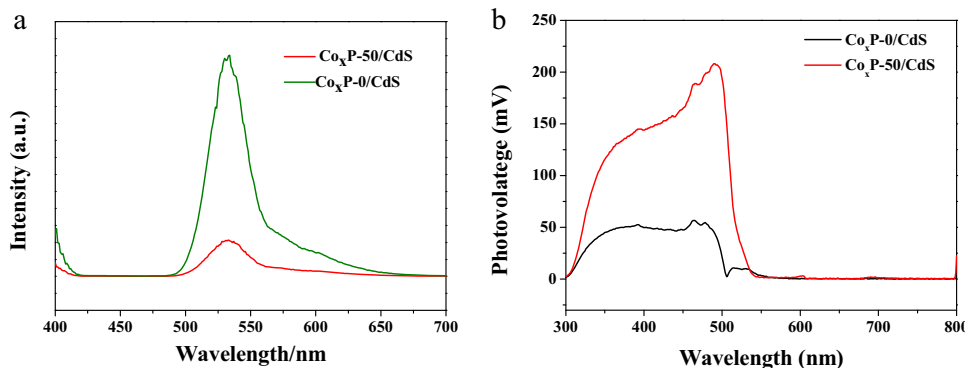


**Fig. 7.** (a) Photoluminescence spectra of  $\text{Co}_x\text{P-0/CdS}$  and  $\text{Co}_x\text{P-50/CdS}$  dispersed in mixture of 3 mL  $\text{H}_2\text{O}$  and 2 mL methanol, and the excitation wavelength was 385 nm. (b) SPV of  $\text{Co}_x\text{P-0/CdS}$  and  $\text{Co}_x\text{P-50/CdS}$ .

ily reduce  $\text{H}^+$  and lead to  $\text{H}_2$  evolution [22,27], and the  $\text{Na}_2\text{S}$  and  $\text{Na}_2\text{SO}_3$  were consumed by photogenerated holes [22,32].

#### 4. Conclusions

In conclusion, taking  $\text{Co}_x\text{P}/\text{CdS}$  as a case, the photochemical rapid preparation of metal phosphides was realized. The obtained  $\text{Co}_x\text{P}/\text{CdS}$  composite is proved as highly robust sunlight-driven HER photocatalyst, due to the efficient transfer of photogenerated electrons as well as excellent catalytic hydrogen production performance of  $\text{Co}_x\text{P}$ . This work provides a novel method for the preparation of metal phosphides as HER cocatalyst in photocatalysis, which is safe and energy-saving. In addition, the photochemical synthesis route proposed in our work could open a door for facile preparation and practical application of many other metal phosphides.

#### Acknowledgements

The authors gratefully acknowledge the support from the National Natural Science Foundation of China (No. 21676123, 21575052, 21275065), the Natural Science Foundation of Jiangsu Province (No. BK20161127), the Fundamental Research Funds for the Central Universities (JUSRP51623A), the Opening Foundation of Shandong Provincial Key Laboratory of Clean Production of Fine Chemicals (ZDSYS-KF201504) from Shandong Normal University and MOE & SAEA for the 111 Project (B13025). The authors also thank Dr. Jinze Lv for his kind help on SPV technology.

#### Appendix A. Supplementary data

Supplementary data associated with this article can be found, in the online version, at <http://dx.doi.org/10.1016/j.apcatb.2017.03.076>.

#### References

- [1] A. Fujishima, K. Honda, *Nature* 238 (1972) 37–38.
- [2] J. Liu, Y. Liu, N. Liu, Y. Han, X. Zhang, H. Huang, Y. Lifshitz, S. Lee, J. Zhong, Z. Kang, *Science* 347 (2015) 970–974.
- [3] X. Zou, Y. Zhang, *Chem. Soc. Rev.* 44 (2015) 5148–5180.
- [4] P. Zhou, J. Yu, M. Jaroniec, *Adv. Mater.* 26 (2014) 4920–4935.
- [5] P. Liu, J.A. Rodriguez, *J. Am. Chem. Soc.* 127 (2005) 14871–14878.
- [6] J. Kibsgaard, C. Tsai, K. Chan, J.D. Benck, J.K. Nørskov, F. Abild-Pedersen, T.F. Jaramillo, *Energy Environ. Sci.* 8 (2015) 3022–3029.
- [7] Y. Shi, B. Zhang, *Chem. Soc. Rev.* 45 (2016) 1529–1541.
- [8] Y. Xu, R. Wu, J. Zhang, Y. Shi, B. Zhang, *Chem. Commun.* 49 (2013) 6656–6658.
- [9] J.F. Callejas, J.M. McEnaney, C.G. Read, J.C. Crompton, A.J. Biacchi, E.J. Popczun, T.R. Gordon, N.S. Lewis, R.E. Schaak, *ACS Nano* 8 (2014) 11101–11107.
- [10] J. Tian, Q. Liu, A.M. Asiri, X. Sun, *J. Am. Chem. Soc.* 136 (2014) 7587–7590.
- [11] E.J. Popczun, C.G. Read, C.W. Roske, N.S. Lewis, R.E. Schaak, *Angew. Chem. Int. Ed.* 53 (2014) 5427–5430.
- [12] Z. Huang, Z. Chen, Z. Chen, C. Lv, M.G. Humphrey, C. Zhang, *Nano Energy* 9 (2014) 373–382.
- [13] Q. Liu, J. Tian, W. Cui, P. Jiang, N. Cheng, A.M. Asiri, X. Sun, *Angew. Chem. Int. Ed.* 53 (2014) 6710–6714.
- [14] E.J. Popczun, J.R. McKone, C.G. Read, A.J. Biacchi, A.M. Wiltrot, N.S. Lewis, R.E. Schaak, *J. Am. Chem. Soc.* 135 (2013) 9267–9270.
- [15] A.B. Laursen, K.R. Patraju, M.J. Whitaker, M. Retuerto, T. Sarkar, N. Yao, K.V. Ramanujachary, M. Greenblatt, G.C. Dismukes, *Energy Environ. Sci.* 8 (2015) 1027–1034.
- [16] X. Wang, Y.V. Kolen'ko, L. Liu, *Chem. Commun.* 51 (2015) 6738–6741.
- [17] Y. Shi, Y. Xu, S. Zhuo, J. Zhang, B. Zhang, *ACS Appl. Mater. Interfaces* 7 (2015) 2376–2384.
- [18] Z. Xing, Q. Liu, A.M. Asiri, X. Sun, *Adv. Mater.* 26 (2014) 5702–5707.
- [19] J. Tian, Q. Liu, N. Cheng, A.M. Asiri, X. Sun, *Angew. Chem. Int. Ed.* 53 (2014) 9577–9581.
- [20] S. Cao, Y. Chen, C.J. Wang, P. He, W.F. Fu, *Chem. Commun.* 50 (2014) 10427–10429.
- [21] S. Cao, Y. Chen, C.J. Wang, X.J. Lv, W.F. Fu, *Chem. Commun.* 51 (2015) 8708–8711.
- [22] Z. Sun, H. Zheng, J. Li, P. Du, *Energy Environ. Sci.* 8 (2015) 2668–2676.
- [23] S. Cao, Y. Chen, C.C. Hou, X.J. Lv, W.F. Fu, *J. Mater. Chem. A* 3 (2015) 6096–6101.
- [24] Z. Sun, H. Chen, Q. Huang, P. Du, *Catal. Sci. Technol.* 5 (2015) 4964–4967.
- [25] Z. Sun, B. Lv, J. Li, M. Xiao, X. Wang, P. Du, *J. Mater. Chem. A* 4 (2016) 1598–1602.
- [26] H. Cheng, X. Lv, S. Cao, Z. Zhao, Y. Chen, W. Fu, *Sci. Rep.* 6 (2016) 19846.
- [27] W. Bi, L. Zhang, Z. Sun, X. Li, T. Jin, X. Wu, Q. Zhang, Y. Luo, C. Wu, Y. Xie, *ACS Catal.* 6 (2016) 4253–4257.
- [28] H. Zhao, Y. Dong, P. Jiang, H. Miao, G. Wang, J. Zhang, *J. Mater. Chem. A* 3 (2015) 7375–7381.
- [29] J.S. Jang, U.A. Joshi, J.S. Lee, *J. Phys. Chem. C* 111 (2007) 13280–13287.
- [30] F.H. Saadi, A.I. Carim, E. Verlage, J.C. Hemminger, N.S. Lewis, M.P. Soriaga, *J. Phys. Chem. C* 118 (2014) 29294–29300.
- [31] Z. Sun, Q. Yue, J. Li, J. Xu, H. Zheng, P. Du, *J. Mater. Chem. A* 3 (2015) 10243–10247.
- [32] H. Zhao, Y. Dong, P. Jiang, G. Wang, H. Miao, R. Wu, L. Kong, J. Zhang, C. Zhang, *ACS Sustain. Chem. Eng.* 3 (2015) 969–977.
- [33] L. Bi, D. Xu, L. Zhang, Y. Lin, D. Wang, T. Xie, *Phys. Chem. Chem. Phys.* 17 (2015) 29899–29905.
- [34] L. Kong, Y. Dong, P. Jiang, G. Wang, H. Zhang, N. Zhao, *J. Mater. Chem. A* 4 (2016) 9998–10007.
- [35] J. Chang, Y. Xiao, M. Xiao, J. Ge, C. Liu, W. Xing, *ACS Catal.* 5 (2015) 6874–6878.
- [36] A.P. Grosvenor, S.D. Wik, R.G. Cavell, A. Mar, *Inorg. Chem.* 44 (2005) 8988–8998.
- [37] P. Jiang, Q. Liu, C. Ge, W. Cui, Z. Pu, A.M. Asiri, X. Sun, *J. Mater. Chem. A* 2 (2014) 14634–14640.